Physica Medica 57 (2019) 238–244

Contents lists available at ScienceDirect

Physica Medica

journal homepage: www.elsevier.com/locate/ejmp

Original paper

# Moving across the static magnetic field of a 1.5 T MRI scanner: Analysing compliance with Directive 2013/35/EU

Davide Gurrera[a,*], Karmenos K. Gallias[b], Marco Spanò[b], Boris F. Abbate[b], Francesca D'Alia[b], Giuseppina Iacoviello[b], Vittorio Caputo[b]

[a] Università degli Studi di Palermo, Dipartimento di Fisica e Chimica, Viale delle Scienze Ed. 18, 90128 Palermo, Italy
[b] A.R.N.A.S. Civico Di Cristina Benfratelli, U.O.C. Fisica Sanitaria, Piazza Nicola Leotta 4, 90127 Palermo, Italy

ARTICLE INFO

*Keywords:*
MRI
Exposure
Safety
NIR

ABSTRACT

Does the exposure of magnetic resonance imaging personnel to static magnetic fields fully comply with Directive 2013/35/EU? Despite the obligation to satisfy this question, a general answer cannot be provided, nor are final satisfying good practices methods for exposure assessment currently available. In order to contribute to fix this problem, three different 1.5 T scanners are analysed and – by a new theoretical insight – a positive answer is provided.

## 1. Introduction

At the time of writing, the deadline to transpose into national laws the Directive 2013/35/EU adopted by the European Parliament and the Council of the European Union concerning "the exposure of workers to the risks arising from physical agents" [1] is long past [2], but still final satisfying good practices methods for exposure assessment are not at hand, particularly when considering risks arising for magnetic resonance imaging (MRI) personnel moving across the permanent static magnetic field straying from the scanner, which is the matter of the study here presented.

The Directive states the following.

> Article 3(2)
> Member States shall require that employers ensure that the exposure of workers to electromagnetic fields is limited to the health effects ELVs and sensory effects ELVs[1] […].

> Article 4(2)
> […] the employer shall identify and assess electromagnetic fields at the workplace, taking into account the relevant practical guides referred to in Article 14 and other relevant standards or guidelines provided by the Member State concerned, including exposure databases.

> Article 4(3)
> If compliance with the ELVs cannot be reliably determined on the basis of readily accessible information, the assessment of the exposure shall be carried out on the basis of measurements or calculations. In such a case, the assessment shall take into account uncertainties concerning the measurements or calculations, such as numerical errors, source modelling, […].

However, the two volumes of the "Non-binding guide to good practice for implementing Directive 2013/35/EU" by the European Commission referred to in the Directive [3,4], and studies therein [5–8], do not definitely bridge the gap between regulation and implementation. Therefore, in order to contribute to fix this problem, compliance with the Directive is now examined for three different scanners.

## 2. The physics of the problem

### 2.1. The (fundamental) role of the Loretz' force

Let $\gamma(t)$ be an oriented closed conducting wire moving across a static magnetic field $\vec{B}_{\text{ext}}$, $\vec{v}$ the velocity of each point of the wire, $S_{\gamma(t)}$ an arbitrary surface enclosed by $\gamma(t)$.

Then, according to the Faraday-Neumann's law:

* Corresponding author.
*E-mail address:* davide.gurrera@unipa.it (D. Gurrera).

[1] The acronym ELVs stands for exposure limit values, i.e. "values established on the basis of biophysical and biological considerations, in particular on the basis of scientifically well-established short-term and acute direct effects". In particular, (i) Health effects ELVs: "ELVs above which workers might be subject to adverse health effects, such as thermal heating or stimulation of nerve and muscle tissue"; (ii) Sensory effects ELVs: "ELVs above which workers might be subject to transient disturbed sensory perceptions and minor changes in brain functions" (as defined in Article 2 of the Directive).

https://doi.org/10.1016/j.ejmp.2018.11.004
Received 10 July 2018; Received in revised form 13 September 2018; Accepted 6 November 2018
Available online 20 November 2018

$$\oint_{\gamma(t)} \vec{E}\cdot\hat{t}\,dl = -\iint_{S_{\gamma(t)}} \frac{\partial\vec{B}}{\partial t}\cdot\hat{n}\,dS \tag{1}$$

or equivalently:

$$\oint_{\gamma(t)} (\vec{E} + \vec{v}\times\vec{B})\cdot\hat{t}\,dl = -\frac{d}{dt}\iint_{S_{\gamma(t)}} \vec{B}\cdot\hat{n}\,dS \tag{2}$$

where $\vec{E}$ and $\vec{B}$ are the electric field and the *overall* magnetic field, respectively. The rest of the notation is assumed to be familiar to the Reader.

A glance at Eq. (1) provides ready and invaluable information. If the inductance of the wire is negligible, then it is possible to assume that $\vec{B} = \vec{B}_{ext}$ and there is no time dependence. Therefore, the generated electric field comes out to be irrotational and – as a consequence – has to be caused *only* by a continuous charge redistribution within the wire. And such a redistribution is imposed by the action of the Loretz' force.

The complete cause and effect picture is as follows. Free charges within the conductor start moving across the external magnetic field with a *mean* velocity that – at each point – is equal to the velocity of the wire. Then the Lorentz' force accelerates them and causes a charge separation that produces an electrostatic field $\vec{E}$ opposing further accumulation, i.e. opposing the *electromotive field* $\vec{v}\times\vec{B}$.

Except for particular given arrangements of $\vec{B}_{ext}$ and $\vec{v}$, equilibrium is not reached and a time-varying density current $\vec{J}$ flows along the wire:

$$\vec{J} = \sigma(\vec{E} + \vec{v}\times\vec{B}), \tag{3}$$

where $\sigma$ is the electrical conductivity. Then, indicating by $R$ the electrical resistance, the current $i$ may be obtained directly as

$$i = \frac{\oint_{\gamma(t)} \vec{v}\times\vec{B}\cdot\hat{t}\,dl}{R}. \tag{4}$$

As far as the magnetic field produced by the induced current may be neglected, there will be only an *electromotive field* $\vec{v}\times\vec{B}$ and a reaction electrostatic field ($\nabla\times\vec{E} = \vec{0}$). And in such a case, in order to calculate the electromotive force and the current, there is no need to make use of the rate of change of the magnetic flux (Eq. (4)).

### 2.2. Focusing the compliance problem

Compliance with the Directive in the case of movement within the static magnetic field of a 1.5 T scanner will require the "electric field" generated inside the body of the exposed subject to be lower than the health effects ELVs and sensory effects ELVs (see Annex II in [1]) as reported in Tables 1 and 2, respectively. The health effects ELVs are spatial peak values *in the entire body*, while the sensory effects ELVs are spatial peak values *only in the head*. In both cases, $f$ is the frequency of the motion-induced "electric field".

Now, a human body moving inside an MRI room may be considered as a special instance of a massive extended non-ferromagnetic conductor for which all the reasoning developed in the previous paragraph applies. Particularly, the motion-induced "electric field" to be tested against the ELVs will be the sum of the *electromotive field* $\vec{v}\times\vec{B}$ and the reaction electrostatic field $\vec{E}$. If the latter – which even a computational model accounting for the electrical properties of the human body could only approximate – is neglected, then an overestimation of the induced field may be expected. But that even results in a precautionary approach.

**Table 1**
Health effects ELVs for internal electric field strength.

| Frequency range | Health effects ELVs |
|---|---|
| 1 Hz ⩽ f < 3 kHz | 1.1 V m$^{-1}$ |

**Table 2**
Sensory effects ELVs for internal electric field strength.

| Frequency range | Sensory effects ELVs |
|---|---|
| 1 Hz ⩽ f < 10 Hz | 0.7/f V m$^{-1}$ |

### 2.3. Source modelling

Providing a source model able to yield an "exact" map of the stray $\vec{B}$ field around the scanner (necessary to determine the electromotive $\vec{v}\times\vec{B}$) would certainly be "beyond the capability of most institutions carrying out routine MRI procedures" [3]. Indeed, such a model would require taking into account the particular optimization design of the considered magnet and even the hosting room (inter alia [9,10] and references therein). A different approach is then proposed.

Despite the particular kind of shielding technique, most of MRI systems consist of cylindrical superconducting solenoids generating a clinical magnetic field $\vec{B}_{int}$ aligned in the axial direction. Then, let $L$ be the length of the magnet, $n$ the number of coils per unit length, $S$ the area of each of them, $i$ the circulating current. In the central volume, the two following are expected to apply:

$$B_{int} = \mu_0 ni \tag{5}$$

$$m = nLiS = \frac{B_{int}}{\mu_0}LS, \tag{6}$$

where $\mu_0$ is the vacuum permeability and $m$ is the modulus of the (total) generated magnetic dipole. The shielding being neglected, for the stray field at point $\vec{r}$ outside the scanner (far distant from the centre of the magnet) the following may be assumed to hold:

$$\vec{B}(\vec{r}) = -\frac{\mu_0}{4\pi}\nabla\frac{\vec{m}\cdot\vec{r}}{r^3}, \tag{7}$$

where the only unknown – the origin of $\vec{r}$ (the location of the magnetic dipole) – can be estimated by fitting the modulus against a suitable set of measured values and may be reasonably expected to provide the necessary degrees of freedom to account for the particular stray field lines even in presence of the unknown shielding design.

## 3. Instrumentation and measures

### 3.1. Preliminary estimations

The compliance assessment technique introduced in the previous section has been applied to three different (by model and/or manufacturer) 1.5 T scanners hereafter referred to as Machine A, B and C, and for each of them shown in Table 3 are the modulus of the generated magnetic dipole and its height above the floor level as obtained by making use of available basic information and Eq. (6), where $L$ and $S$ are considered to be the length of the bore and the area of its aperture, respectively. However, because of such a black box estimation – obtained disregarding the actual magnet structure – the values reported in the table are to be regarded only as a reasonable approximation useful to reduce the number of degrees of freedom in the model, the free parameters being expected to compensate for the lack of precise estimation. Were it not the case, then the height and the modulus of $\vec{m}$ would be added to the fitting optimization process.

**Table 3**
Height above floor level (m) and modulus $m$ (MA m$^2$) of the generated magnetic dipole.

| | Machine A | Machine B | Machine C |
|---|---|---|---|
| $m$ | 0.60 | 0.54 | 0.44 |
| Height | 1.00 | 1.07 | 1.00 |

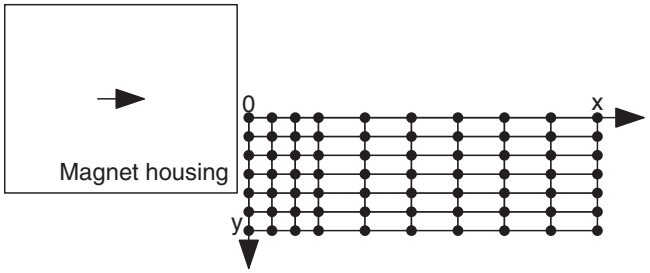


**Fig. 1.** The modulus of the stray field has been measured in each of the indicated points and at each of three different heights. The short and long steps in the net are 20 and 40 cm long, respectively. The map lies as close as possible to the bore and the couch. The arrow inside the magnet housing indicates the magnetic dipole.

### 3.2. Mapping the stray field

Providing an adequate measure of the stray field outside each scanner has instead required – unsurprisingly – a great deal of effort.

By making use of a three-axis hall magnetometer, the *modulus* of the magnetic field has been measured according to the map shown in Fig. 1, positioned as close as possible to the bore and the couch and whose short and long steps are 20 and 40 cm long, respectively. Particularly, measures have been recorded in each of the 70 indicated points and at each of three different heights from the floor level: 72, 119 and 156 cm. Therefore, a three-dimensional map composed of 210 measures has been produced for each scanner, the major issue being represented by the dispersion of the values in proximity of the magnet. In fact, a slight mispositioning of the probe would result in severe misleading estimations. In order to control them, a twofold measurement procedure has been applied:

(i) for each point in the map the magnetometer was set to provide an average of 1000 instantaneous measures;
(ii) in the "fine" part of the net the probe was allowed to move in the neighbourhood of each point and the obtained values were used to provide a suitable plus-minus range.

As a result, each measure in the sample is associated to a position dependent uncertainty up to 50 mT.

### 3.3. Implementation

What follows has been carried out in the R environment for statistical computing and visualisation [11] by self-developed code.

## 4. Results

### 4.1. The fit

If the dipole field in (7) is going to provide an adequate representation of the magnetic field *outside* the scanner, then its modulus is expected – after a fitting optimization process – to conform to the measured values of the three-dimensional map described in the previous section. The two unknowns to be estimated by the nonlinear regression [12] are the distance along the x and y directions in Fig. 1 of the magnetic dipole (the arrow inside the magnet housing) from the origin of the coordinate system and in Table 4 are the values obtained for the three analysed cases.

The reported estimations – of course – cannot be checked against a *true value*, since the position of the exploited dipole is unknown, but still they pass a first goodness-of-fit test. In fact, in each of the three cases the values are in agreement with those imposed by the magnet housing.

**Table 4**
Distance (cm) along the x and y directions in Fig. 1 of the magnet isocenter from the origin of the coordinate system, as estimated by the fit search.

| | Machine A | Machine B | Machine C |
|---|---|---|---|
| $\Delta x$ | 76 | 73 | 56 |
| $\Delta y$ | 9 | 4 | −2 |

And that is far from being a priori obvious. Indeed, adding the height and modulus of $\vec{m}$ to the pool of free parameters – without proper constraints – would in general lead to unacceptable results, which justifies the performed preliminary estimations. And in a roundabout way those estimations are somehow confirmed by the obtained results.

However, a deeper insight is provided by comparing for each point the measured value against that predicted by the suggested model and in Fig. 2 results from Machine A are shown. Particularly, on the left is the modulus of the stray field as provided by (7) at each of the three considered heights from the floor level, on the right the absolute value of the difference between the raw measures as provided by the magnetometer, without any position tolerance/correction (see Section 3), and the corresponding predicted values. As expected, discrepancy grows near the bore – where it is approximately 90 mT – and fades away from it. However, a more reliable range than that shown in the figure is obtained when tolerance due to measurement uncertainty is introduced, with the maximum difference approaching in this case 50 mT.

But going still further, the deepest insight and a final quantitative goodness-of-fit test is provided by the residuals analysis reported in Fig. 3 displaying the scatter plot of all the estimated $B$ values versus the raw measures. Also displayed in the figure are two almost coincident straight lines. Particularly, the black one is the best fit line, while the other represents "perfect" modelling, i.e. $y = x$. As a result, despite the inherent heteroscedasticity, adherence to the black line, as measured by the Pearson's correlation coefficient, is 0.97.

Results for the other examined machines do not differ significantly and are omitted for brevity. In particular, discrepancy lies within the same range.

### 4.2. Assessing the whole-body exposure

Now that a model for the static stray $\vec{B}$ field tuned to the particular examined environments has been gained, in order to compute the motion-induced $\vec{v} \times \vec{B}$ field necessary to assess the exposure, reliable assumptions about the involved velocities are to be made. Here, a conservative approach will be adopted according to which the MRI operator will be supposed moving at a speed of 1.5 m s $^{-1}$, which – over the short distances involved – is considerably above the average [13]. Moreover, an unrealistic (but again conservative) steady-state speed will be assumed from the first up to the very last step.

With the above in mind, the following three scenarios are examined:

(i) Scenario A: movement across the whole MRI room towards the bore along the x direction;
(ii) Scenario B: towards the couch along the y direction;
(iii) Scenario C: towards the bore/couch along the x-y direction.

Results for each of the three examined machines are shown in Fig. 4 where the maps of $|\vec{v} \times \vec{B}|$, at the height of the magnetic dipole (i.e. where $B$ is maximum), are displayed. The coordinate system is the same as that in Figs. 1 and 2, and the origin – even if its exact position cannot be given – is so close to the scanner housing and the couch (only a few centimetres apart) that an operator could not stand at that point.

The motion-induced *electric* field comes out to be lower than the

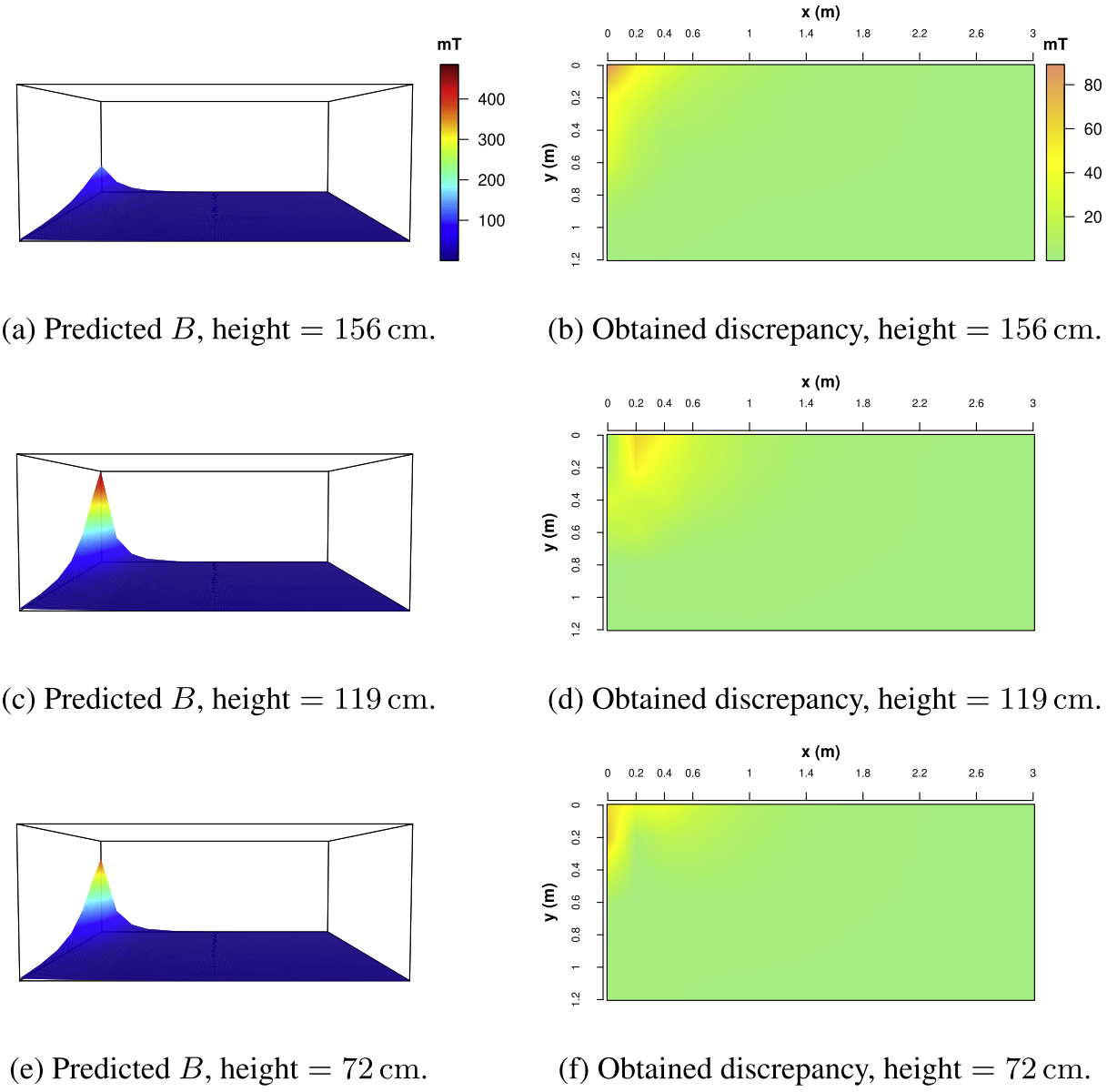


(a) Predicted $B$, height $= 156\,\mathrm{cm}$.

(b) Obtained discrepancy, height $= 156\,\mathrm{cm}$.

(c) Predicted $B$, height $= 119\,\mathrm{cm}$.

(d) Obtained discrepancy, height $= 119\,\mathrm{cm}$.

(e) Predicted $B$, height $= 72\,\mathrm{cm}$.

(f) Obtained discrepancy, height $= 72\,\mathrm{cm}$.

**Fig. 2.** For Machine A, on the left the modulus of the stray field as determined by (7) at each of the three considered heights from the floor level, on the right the absolute value of the difference between the predicted and the raw measured values. Refer to Fig. 1 as for the coordinate system.

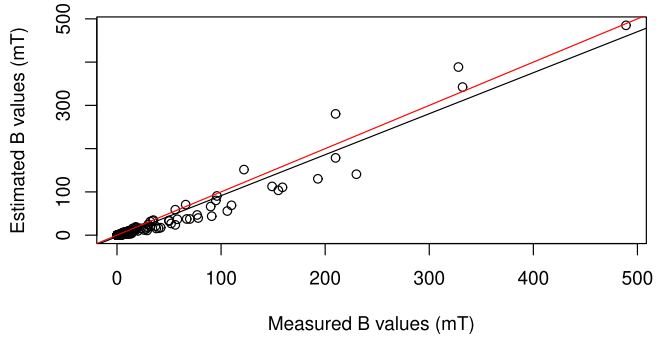


**Fig. 3.** For Machine A, scatter plot of all the 210 values of $B$ estimated by (7) versus the raw measures. The black straight line shows the best fit, while the other represents "perfect" modelling, i.e. $y = x$.

health effects ELV (see Table 1) and to such an extent that compliance with the Directive could not be affected even by the discrepancy observed in the fit. Moreover, results appear to be machine-independent.

### 4.3. Assessing the head exposure

According to the results depicted in Fig. 4, Scenario B appears to be the riskiest and therefore compliance with the ELV for the sensory effects (Table 2) will be assessed only for that case. Such an assessment will require this time evaluating the electromotive field at the level of the head and as a function of time, the inherent frequency being used to adjust the proper signal-dependent threshold.

Following the above, results for the three examined scanners are shown in Fig. 5, where – by the usual conservative approach – a height of 160 cm has been chosen for the head. Particularly, the coloured lines provide the modulus of the motion-induced field during the movement *next to the magnet* of an operator starting at $y_0 = +1.2$ m (refer to Fig. 2) and reaching the bore aperture by a constant speed of $1.5\,\mathrm{m\,s^{-1}}$ (therefore, the motion lasts 0.8 s), the dashed line indicates the corresponding exposure threshold which is practically the same for the three examined machines. In fact, as shown in Table 5, the motion-related frequencies are almost equal, resulting in a common ELV approximately of $0.42\,\mathrm{V\,m^{-1}}$. And these frequencies – which are intended to

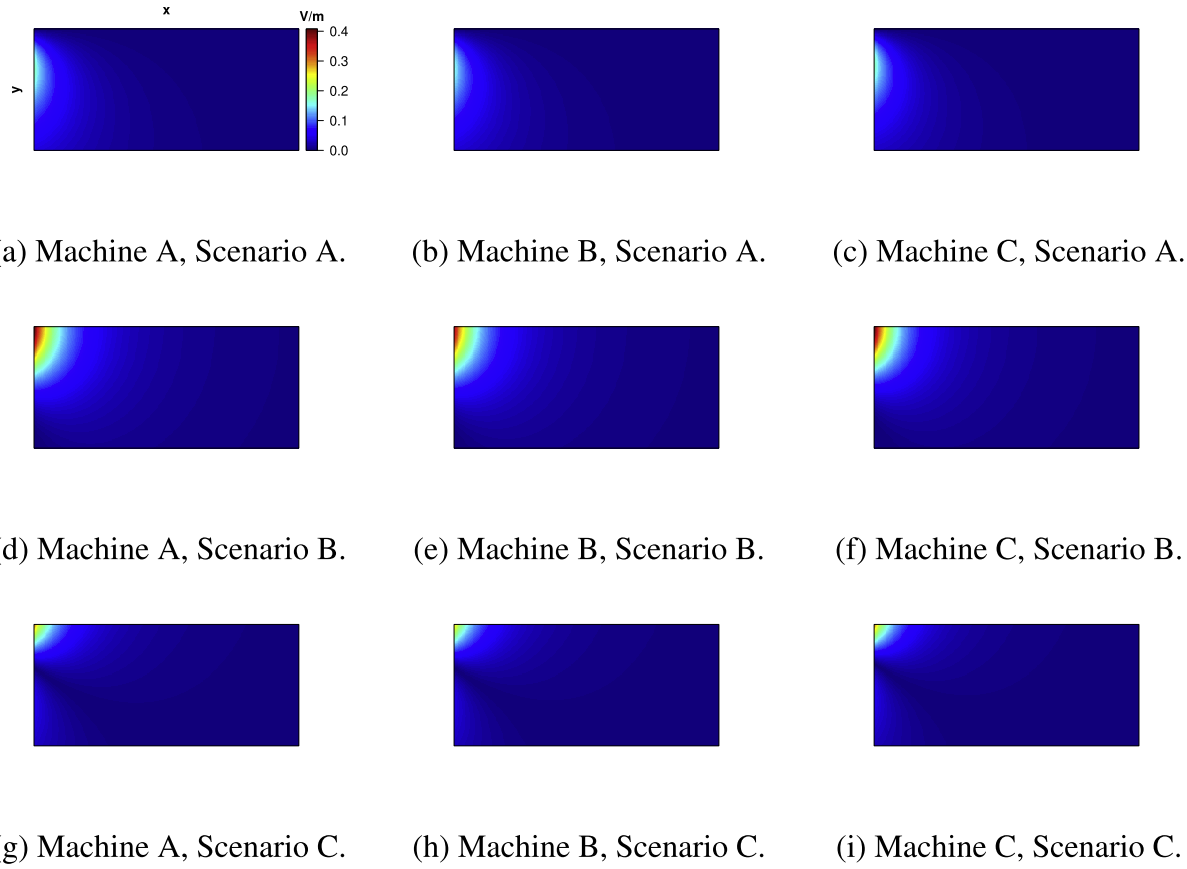


(a) Machine A, Scenario A. (b) Machine B, Scenario A. (c) Machine C, Scenario A.

(d) Machine A, Scenario B. (e) Machine B, Scenario B. (f) Machine C, Scenario B.

(g) Machine A, Scenario C. (h) Machine B, Scenario C. (i) Machine C, Scenario C.

**Fig. 4.** Modulus of $\vec{v} \times \vec{B}$ at the height of the magnetic dipole for each of the three considered machines and for each of three analysed scenarios: (i) Scenario A: $\vec{v} = (-1.5\,\mathrm{m\,s^{-1}},\ 0)$; (ii) Scenario B: $\vec{v} = (0,\ -1.5\,\mathrm{m\,s^{-1}})$; (iii) Scenario C: $\vec{v} = -1.5\,\mathrm{m\,s^{-1}}\ (2^{-1/2},\ 2^{-1/2})$. Refer to Figs. 1 and 2 as for the coordinate system.

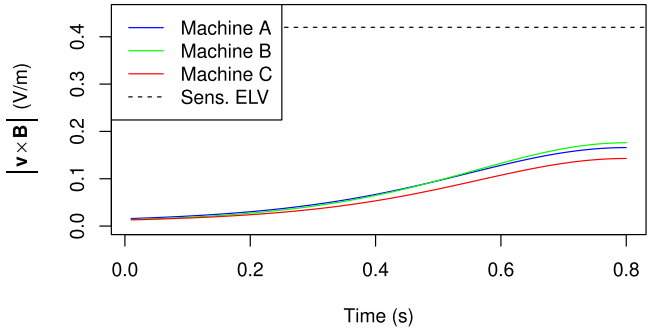


**Fig. 5.** The modulus of the electromotive field induced in the head as a function of time along with the corresponding ELV for the sensory effects.

**Table 5**
Frequency and peak value of the electromotive field induced in the head.

| Machine | $f$ (Hz) | $\lvert\vec{v} \times \vec{B}\rvert_{\max}$ (V m$^{-1}$) |
|---|---|---|
| A | 1.67 | 0.17 |
| B | 1.66 | 0.18 |
| C | 1.65 | 0.14 |

characterize the spectral content of the involved electric signal – have been estimated by the spectral centroid [14] of the corresponding periodogram. Therefore:

$$f = \frac{\sum_i a_i f_i}{\sum_i a_i}, \tag{8}$$

where $f_i$ and $a_i$ are the frequency and the corresponding squared magnitude in the spectral band $i$, respectively.[2]

Again, the motion-induced field – whose maximum values are given in Table 5 – comes out to be far below the ELV and almost machine-independent.

[2] Given $N$ equally time spaced samples of the signals shown in Fig. 5 (conveniently zero-padded)

$$E_{\mathrm{em}}(n) = |\vec{v} \times \vec{B}| = |(0,\ v_y,\ 0) \times (B_x,\ B_y,\ B_z)| = \\ = |v_y| \sqrt{B_x^2(0,\ y_0 + v_y \tfrac{n}{f_s},\ z_h) + B_z^2(0,\ y_0 + v_y \tfrac{n}{f_s},\ z_h)} \\ n = 0,\ 1, \ldots, N-1 \tag{9}$$

indicating by $f_s$ the sampling rate and by $z_h$ the z-coordinate of the head, the power at frequency

$$f_i = \frac{i}{N} f_s \qquad i = 1,\ 2,\ \ldots,\ N/2 \tag{10}$$

is given by the Discrete Fourier Transform

$$a_i \propto \left| \sum_{n=0}^{N-1} W_n\, E_{\mathrm{em}}(n)\, e^{-j\,2\pi\, n\, \frac{f_i}{f_s}} \right|^2 \tag{11}$$

$j$ being the imaginary unit and $W_n$ a convenient tapering window [15].

### 4.4. Going faster

But how fast is an MRI operator allowed to move?

Because of the approximations involved in the model, answering this question is not strictly correct, but – nonetheless – it will provide further information. That specified, as for the health ELV an operator would exceed it only if running (at approximately $4\,m\,s^{-1}$), while the more restrictive threshold related to the sensory effects would be reached at $2.3\,m\,s^{-1}$ (when the electromotive field frequency would be 2.6 Hz).

## 5. Discussion

Before providing in the next concluding section the compliance statement for the three machines analysed in this work, its contribution needs to be fixed, since a few remarks are still in order.

In a nutshell:

(i) it is possible to estimate the induced field inside the body of the MRI operator without any particular human model, simply by making use of the electromotive field $\vec{v} \times \vec{B}$;
(ii) a magnetic dipole may provide a parsimonious, but still adequate, 3D map of the magnetic field straying from the scanner, its specific architecture details being ignored;
(iii) the developed framework may be used to analyse the effect of any kind of motion, including rotations and up/down movements.

*Point i.* Now, of the three above, it is particularly the first point that deserves attention since – definitely surprisingly – it has been so far somehow missed. And to this regard it is paradigmatic the following comment of Gowland P. and Glover P. [16] on ICNIRP[3] guidelines for limiting exposure to electric fields induced by movement of the human body in a static magnetic field and by time-varying magnetic fields below 1 Hz [17].

> However, we are keen to point out that there was a more serious problem with using that data in this way. At the time we wrote the paper,[4] we proposed that the dominant mechanism was induced electric currents. However, as ICNIRP noted in the new guidelines, this mechanism has been questioned by Roberts, who proposed a Lorentz force mechanism [19]. […].
>
> We have now carried out further studies that support Roberts' Lorentz force mechanism [20–22]. Furthermore, the new mechanism explains the previously anomalous observation of apparent vertigo-type effects in small rodents, which are physically too small to be able to develop sufficient current densities in their heads to cause nerve excitation [23].
>
> It now seems likely that the perceptual effects of the changing Lorentz force are the primary reason why movement causes vertigo.

Indeed – as discussed in Section 2 – as long as $\frac{\partial \vec{B}}{\partial t} = \vec{0}$, there will be only the electromotive field $\vec{v} \times \vec{B}$ and an irrotational reaction field $\vec{E}$. Saying it differently, moving in a static not-uniform magnetic field is not equivalent to stay (fixed) in a time-varying $\vec{B}$. In fact, in the second case there would be only a rotational $\vec{E}$ (no charge separation) and no electromotive field (i.e. no Lorentz mechanism).

*Point ii.* However, the electromotive field will provide the required *punctual* information, provided that *punctual* information of the *vector* $\vec{B}$ (direction and modulus) is available. And here, as a second contribution, it is showed that a simple magnetic dipole might serve the purpose. At least, it did in the three examined cases. An "exact" map – while requiring too demanding ad hoc models – would not provide better answers. In fact, in order to provide a compliance statement the determined exposure values need to be far below the prescribed limits.

It is acknowledged – however – that this point would benefit from further investigation on other different machines.

*Point iii.* Finally, the approach here proposed for assessing compliance with the Directive additionally allows to analyse the effect of any kind of motion one might envisage, with no impracticable computing effort. Particularly, acceleration could be included along with the aforesaid rotations and up/down movements.

However, as long as the interest is limited to a compliance statement, the number of informative scenarios might reduce, as it was the case with the machines here analysed, the obtained results excluding the necessity to investigate any further.

## 6. Conclusions

The developed assessment method, once run on the three *different* 1.5 T machines here analysed, has yielded a shared final positive compliance statement: no risk to exceed both the health and sensory effects ELVs.

And the strong similarity in the results suggests that the same might apply to each 1.5 T MRI facility.

## Conflicts of interest

None.

## References


[1] European Union, Directive 2013/35/EU of the European Parliament and of the Council of 26 June 2013 on the minimum health and safety requirements regarding the exposure of workers to the risks arising from physical agents (electromagnetic fields) (20th individual Directive within the meaning of Article 16(1) of Directive 89/391/EEC) and repealing Directive 2004/40/EC. Official Journal of the European Union 2013;56(179).

[2] Morega M, Calotă VC. From Directive 2013/35/EU to national legislation: transposition, implementation and assessment work. 2016 International Conference on Applied and Theoretical Electricity (ICATE). 2016. p. 1–6.

[3] Directorate-General for Employment, Social Affairs and Inclusion (European Commission), Non-binding guide to good practice for implementing Directive 2013/35/EU – Volume 1: Practical Guide; 2016.

[4] Directorate-General for Employment, Social Affairs and Inclusion (European Commission). Non-binding guide to good practice for implementing Directive 2013/35/EU – Volume 2: Case Studies; 2016.

[5] Capstick M, McRobbie D, Hand J, Christ A, Kühn S, Hansson Mild K, et al. An Investigation into Occupational Exposure to Electromagnetic Fields for Personnel Working With and Around Medical Magnetic Resonance Imaging Equipment; 2008. URL:http://www.itis.ethz.ch/assets/Downloads/Papers-Reports/Reports/VT2007017FinalReportv04.pdf.

[6] Stam R. The EMF Directive and protection of MRI workers. Possible solutions; 2008. URL:http://www.rivm.nl/dsresource?objectid=9986faba-2db2-4f85-8f27-5d52b3cdbbae&type=org&disposition=inline.

[7] McRobbie DW. Occupational exposure in MRI. Brit J Radiol 2012;85(1012):293–312.

[8] Stam R. The revised electromagnetic fields directive and worker exposure in environments with high magnetic flux densities. Ann Occup Hygiene 2014;58(5):529–41.

[9] Chen X, Steckner M. Electromagnetic computation and modeling in MRI. Med Phys 2017;44(3):1186–203.

[10] Cosmus TC, Parizh M. Advances in whole-body MRI magnets. IEEE Trans Appl Supercond 2011;21(3):2104–9.

[11] R Core Team. R: a language and environment for statistical computing. Vienna, Austria: R Foundation for Statistical Computing; 2018. URL:https://www.R-project.org/.

[12] Baty F, Ritz C, Charles S, Brutsche M, Flandrois JP, Delignette-Muller ML. A toolbox for nonlinear regression in R: the package nlstools. J Stat Software 2015;66(5):1–21. Articles.

[13] Bohannon RW, Williams Andrews A. Normal walking speed: a descriptive meta-analysis. Physiotherapy 2011;97(3):182–9.

[14] Massar M, Fickus M, Bryan E, Petkie D, Terzuoli Jr. A. Fast computation of spectral centroids. Adv Comput Math 2011;35(1):83–97.

[15] Bloomfield P. Fourier analysis of time series: an introduction. John Wiley & Sons, Inc.; 2000.

[16] Gowland P, Glover P. Comment on ICNIRP guidelines for limiting exposure to


[3] The acronym stands for International Commission on Non-Ionizing Radiation Protection.

[4] They refer to [18].

electric fields induced by movement of the human body in a static magnetic field and by time-varying magnetic fields below 1 Hz. Health Phys 2014;107(3):261.
[17] International Commission on Non-Ionizing Radiation Protection. Guidelines for Limiting Exposure to Electric Fields Induced by Movement of the Human Body in a Static Magnetic Field and by Time-Varying Magnetic Fields below 1 Hz. Health Phys 2014;106(3):418–25.
[18] Glover P, Cavin I, Qian W, Bowtell R, Gowland P. Magnetic-field-induced vertigo: a theoretical and experimental investigation. Bioelectromagnetics 2007;28(5):349–61.
[19] Roberts D, Marcelli V, Gillen J, Carey J, Della Santina C, Zee D. MRI magnetic field stimulates rotational sensors of the brain. Curr Biol 2011;21(19):1635–40.
[20] Antunes A, Glover PM, Li Y, Mian O, Day B. Magnetic field effects on the vestibular system: calculation of the pressure on the cupula due to ionic current-induced Lorentz force. Phys Med Biol 2012;57(14):4477–87.
[21] Glover PM, Li Y, Antunes A, Mian O, Day B. A dynamic model of the eye nystagmus response to high magnetic fields. Phys Med Biol 2014;59(3):631–45.
[22] Mian OS, Li Y, Antunes A, Glover P, Day B. On the vertigo due to static magnetic fields. PLoS One 2013;8(10):1–11.
[23] Houpt T, Houpt C. Circular swimming in mice after exposure to a high magnetic field. Physiol Behav 2010;100(4):284–90.